Next Nanotechnology 7 (2025) 100160

Contents lists available at ScienceDirect

Next Nanotechnology

journal homepage: www.sciencedirect.com/journal/next-nanotechnology

Research article

Understanding the synthesis mechanism of arginine functionalized silver/silver chloride nanoparticles using sugar ligands

Şuheda Bolat [a,1], Suna Değirmenci [a,2], Abdurrahman Gümüş [b,3], Zafer Sancak [a,4,*], İdris Yazgan [a,5,*]

[a] Department of Biology, Faculty of Science, Kastamonu University, Türkiye
[b] Department of Electrical and Electronics Engineering, İzmir Institute of Technology, İzmir, Türkiye

ARTICLE INFO

Keywords:
Silver/silver chloride nanoparticles
Sugar ligands
Arginine hydrochloride
Multidrug-resistant *Escherichia coli*

ABSTRACT

In this study, we performed a mechanistic study to understand how the sugar ligand chemistry affected the morphology, size and surface chemistry of Ag/AgCl_NPs synthesized in the presence of L-Arginine hydrochloride and L-Arginine/KCl mixture. The sugar ligands Lactose *p*-methoxyaniline (LMA) and Galactose 5-aminosalicylic acid (G5AS) resulted in formation of sheet-like Ag/AgCl_NPs while Lactose sulfanilic acid (LSA) and Lactose *p*-sulfonyldianiline (LPSA) caused the formation of anisotropic and film-like Ag/AgCl_NPs. The UV-Vis based mechanistic studies showed that the presence of Arginine posed a strong effect on how G5AS and LMA ligands interact with silver ions while the effect was more complicated for the LSA and LPSA ligands due to the fact that they form complexation with Ag^+ ions. The mechanism was further investigated using infrared (IR) studies that showed the increases in Argine and chloride ion concentrations resulted in differentiation of the surface chemistry of the Ag/AgCl_NPs, and appearance of Arginine related IR bands became clearer in the case of co-introduction of Arginine and the sugar ligands. The characterized nanoparticles were then used as antibacterial agent for multidrug resistant *Escherichia coli* species for which less than 10 μM minimum inhibitory concentrations were obtained. The promising antibacterial activity, which could be assigned to the presence of Arginine, was independent from the sugar ligand chemistry and nanoparticles' morphology and size. Particularly, large Ag/AgCl_NP film forming capacity can call further research to be exploited as coating materials for antibacterial application.

1. Introduction

Silver chloride (AgCl) nanoparticles (AgCl_NPs) can find place in a variety of applications, including biological (e.g. antimicrobial, drug delivery etc.), biomedical (e.g. sensing) and industrial (e.g. solar cells) [1]. Various approaches have been applied in the synthesis of AgCl nanoparticles (AgCl_NPs) to obtain benign, reproducible and target-specific properties, which can fall into chemical precipitation methods [2–4], biological methods (e.g. microorganisms) [5] and physical methods [6,7]. Silver nanoparticle (AgNP) formation can take place spontaneously within AgCl_NPs or be induced by physical and/or chemical stimulants [4], hence the abbreviations AgCl_NPs and Ag/AgCl_NPs can refer to each other.

The morphology and size of the nanoparticles can be definitive in their applications [8,9]. AgCl_NPs are generally spherical [3,10], quasi-spherical [6] and irregularly shaped [11], which have been mostly studied for biological applications, such as showing simultaneous anticancer and antibacterial activity [12] and antifungal applications [13]. In addition, sheet-like AgCl_NPs can find applications in catalysis [14], while cubic crystalline AgCl particles can provide superior SERS performance [15]. In addition to stand-alone AgCl_NPs, AgCl crystals (or nanoparticles) can also be synthesized on AgNPs or in composite

* Corresponding authors.
E-mail addresses: zsancak@kastamonu.edu.tr (Z. Sancak), iyazgan@kastamonu.edu.tr (İ. Yazgan).
[1] 0009–0003-6414–9699
[2] 0000–0003-5785–9158
[3] 0000–0003-2993–5769
[4] 0000–0003-1220–9613
[5] 0000–0002-0264–1253

https://doi.org/10.1016/j.nxnano.2025.100160
Received 7 January 2025; Received in revised form 17 February 2025; Accepted 26 March 2025
Available online 4 April 2025

polymers, which can improve catalytic performance (e.g. water splitting) [9,16] or microwave characters [17]. Surface functionalization can provide unprecedented properties in addition to the enhancement of their inherent properties [18]. However, AgCl_NPs were not studied with their surface functionalization, whereas the introduction of the positively charged amino acid Arginine on AgNP has been shown to enhance the stability and biocidal character of the AgNPs [19]. Furthermore, Arginine-stabilized films based on silver nanoparticles can exhibit excellent conductive and adhesive properties [20], and Arginine has also been shown to enhance the film formation of gold nanoparticles [21]. This may be related to the fact that Arginine can enable nanoparticle-nanoparticle interaction resulting in superior antibacterial activity [22], for example its presence in chitosan-gold nanoparticle films improved wound-healing [23].

In this study, carbohydrate derivatives were intended to be used as reducing, capping and stabilizing agents in synthesis of Ag/AgCl_NPs using L-Arginine Hydrochloride, where Arginine was accepted as surface functionalization agent. Sugar ligands can recognize lectins on bacterial surfaces, which phenomenon has been investigated in drug development studies including antibacterial agents and anticancer agents etc. *E.coli* has galectin-1 lectin that can recognize Galactose and its derivatives and play role in bacterial attachment to the mammalian cells [24]. Therefore, we used Lactose (Galactosyl-Glucose) and Galactose derivatives, among which LMA and G5AS ligands can easily reduce Ag^+ ions while LSA and LPSA can form complex with Ag^+ ions. In order to perform a mechanistic understanding of Ag/AgCl_NPs under the experimental conditions, L-Arginine and KCl (as Cl^- ion source) were included in the study. The UV-Vis studies showed that Arginine has great impact on the nanoparticles' morphology and size while IR, HRTEM, SEM and XRD studies along with the UV-Vis studies showed that the characteristics of Ag/AgCl_NPs showed close relationship with the sugar ligands' chemistry. It is known that decoration of nanoparticles' surface with carbohydrates can advance their biological activity [25,26], so a synergistic antibacterial activity was tested as ant antibacterial agent for two Colistin and Carbapenem resistant *E.coli* species, and μg/mL level minimum inhibitory concentration (MIC) and minimum bactericidal concentration (MBC) values were obtained. This is important since drug-resistant bacterial infections not only cause deaths, but also puts a burden on the health-costs [27]. To the best of our knowledge, this is the first study describing how the synthesis of Ag/AgCl_NPs follows a mechanism in the presence of self AgNPs synthesizing and Ag^+ complexing sugar ligands to obtain Arginine functionalized particles.

2. Materials and methods

2.1. Materials

$AgNO_3$, Tryptophane hydrochloride, Tryptophane, KCl, Nutrient Broth, Nutrient Agar and Crystal violet were purchased from Sigma-Aldrich. Pure-water was produced using the Humana Zeneer Pure-water instrument in our labs. TEM grids were from Ted Pella (Cat. Nu 01895-F). Synthesis of the sugar ligands Galactose 5-aminosalicylic acid (G5AS), Lactose methoxyaniline (LMA), Lactose 4,4' sulfonyldianiline (LPSA) and Lactose sulfanilic acid (LSA) can be found in the literature [28].

2.2. Synthesis and characterization of Ag/AgCl nanoparticles

During the synthesis, in all cases, sugar ligand and silver nitrate concentrations were 12.5 and 10 μmol/mL while Arginine, Potassium chloride and Arginine Hydrochloride concentrations were used at 9 μmol/mL except AgNP2s and Arg2 cases for which $AgNO_3$ and Argine concentrations were 20 and 18 μmol/mL. Arg_Cl_Ag/AgCl_NPs refer to Arginine and Potassium chloride were mixed with silver nitrate ions while ArgCl_Ag/AgCl_NPs refer to Arginine Hydrochloride and silver nitrate were mixed for the synthesis. In order to understand the effect of L-Arginine on the interaction between the sugar ligands and Ag(I) ion, a series of experiments were conducted in the absence or presence of chloride ion (KCl was used as Cl^- source), which is shown in Fig. 1.

UV-Vis spectroscopy (Shimadzu UV Pharmaspec 1700), Infrared spectrometer (Bruker ALPHA II Compact FT-IR Spectrometer), High Resolution Transmission Electron Microscopy-Selected Area Diffraction (HRTEM-SAED, service was purchased from the BUMER-Bayburt University of Türkiye, Hitachi at 220 kV), X-Ray Diffraction (XRD, Bruker D8 Advance), Scanning Electron Microscopy- Energy Dispersive X-Ray Analysis (SEM-EDX, Thermo Fisher FEI Quanta FEG 250), and Antibacterial activity characterizations were conducted as described in the literature [22]. For TEM studies, the samples were diluted 20 times and two drops (~20 μL) were placed on TEM grids (TedPella, Product number 01895-F), which were dried for 24 h at room temperature. The SEM-EDX samples were prepared from stock Ag/AgCl_NP solutions by placing 10 μL aliquots on lead-coated copper tape (purchased from local electronics store), which was dried at room temperature for 24 h.

3. Results and discussion

3.1. UV-vis spectroscopic characterization of Ag/AgCl nanoparticles

Fig. 2 shows how different formulations resulted in the formation of colloidal and precipitated AgNPs and Ag/AgCl_NPs. The color of silver nanoparticles is closely related to size and morphology, so the change in color with increasing concentrations of $AgNO_3$ and Arginine and administration of Chloride ions reflects changes in morphology and size. Two of the most dramatic changes were (i) LSA and LPSA sugar ligands did not allow AgNPs to form, whereas addition of Arginine addition to the media allowed rapid formation of AgNPs that even covered the surface of the reaction tubes. It is possible that LSA and LPSA sugar ligands trigger the formation of silver metal organic frameworks or coordination complexes under the experimental conditions, as both have sulfonyl groups [29]. Precipitation of LSA_Arg_Cl_Ag/AgCl_NPs and LPSA_Arg_Cl_Ag/AgCl_NPs showed different patterns compared to Arg_Cl_AgNPs, which could be related to that LSA and LPSA gathered Ag^+ ions and Arginine contributed Ag/AgCl_NPs formation. Precipitation of nanoparticles is closely related to the surface chemistry and size [30]. However, Arg_Cl_Ag/AgCl_NPs gave pale particles, which is a sign of limited Ag^0 presence The other (ii) observation was only G5AS_Cl_Ag/AgCl_NPs gave distinct color in comparison to that LMA, LSA and LPSA sugar ligands did not give any distinct color with or without Arginine presence in sugar ligand_Cl_Ag/AgCl_NPs. The color difference between Arg_Cl_ Ag/AgCl_NPs and ArgCl_Ag/AgCl_NPs could be related to two things (i) there were five-times higher Ag^+ in ArgCl_Ag/AgCl_NPs since the reaction took place in 5 mL while the former one was 1 mL volume, or (ii) the incubation period was one weak for the latter case while that was 3-day for the former case. It should also be mentioned that AgCl_NPs are supposed to be whitish since Ag^+ ions do not turn into metallic Ag^0. However, the presence of Ag^0 within AgCl_NPs results in Ag/AgCl_NPs formation, for which characteristic colors form. Besides, the sugar ligand chemistry has a very strong impact on the color of the metallic nanoparticles that was independent from the characteristics [28]. This observation was similar for the sugar ligand synthesized Ag/AgCl_NPs as well. The UV-Vis spectra showed that the SPR peak of LSA_Ag/AgCl_NPs, LPA_Ag/AgCl_NPs, LMA_Ag/AgCl_NPs and G5AS_Ag/AgCl_NPs were 420 nm, 580 nm, 555 nm and 520 nm, respectively. LSA_Ag/AgCl_NPs also gave wide and non-characteristic SPR peak starting 490 nm. Presence of SPR peak proves that the nanoparticles were not just AgCl_NPs, rather they were in the form of Ag/AgCl_NPs.

In order to understand how presence of Arginine and Chloride ion affected the sugar ligand and silver ion interaction during the Ag/AgCl_NPs synthesis, a series of UV-Vis based studies were conducted (Fig. 3). Hereby, we used L-Arginine and KCl to perform these tests. It is expected that the introduction of Arginine and Arginine hydrochloride

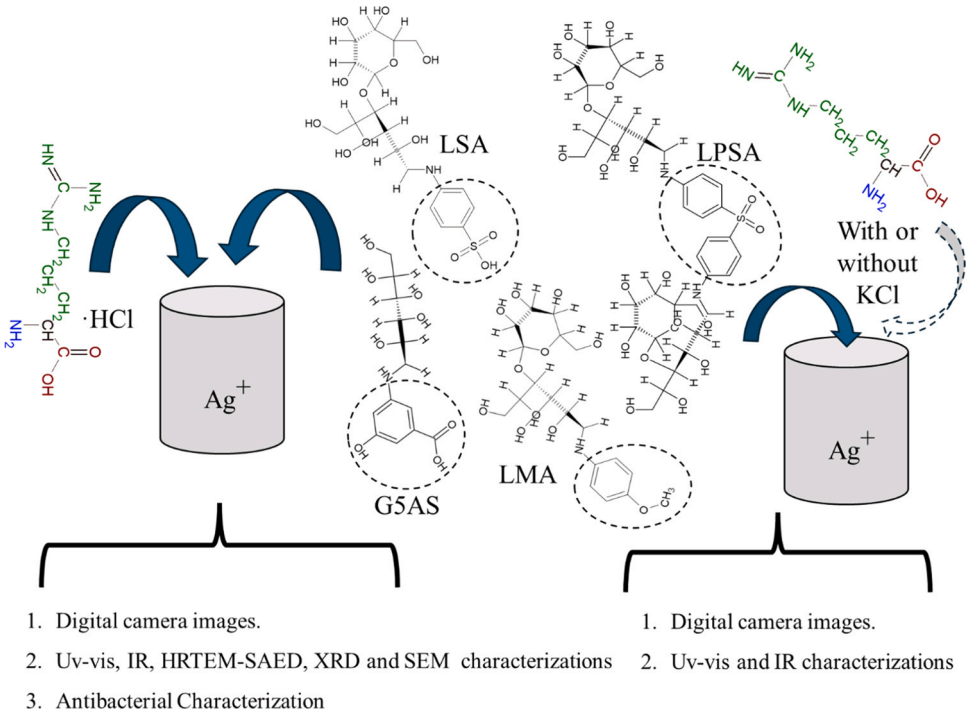

Fig. 1. Flow of the Ag/AgCl nanoparticle synthesis and characterizations.

can differently affect the pH of the reaction medium, which may alter the reaction kinetics. When we checked the reaction mediums using pH paper, 0.45 mM Arginine hydrochloride or Arginine made the reaction mediums' pH ~4.5–5.5 and ~6.0–7.0 depending on the sugar ligand. Previous studies showed that this much pH alteration did not pose any significant effect on the AgNPs formation kinetics and morphology [31]. Besides, structure of Argine are quite similar at these pH ranges [32], so it is possible to claim that the experiments were conducted under similar conditions. Both phenyl ring [33] and sugar moieties [25,34,35] can interact with metallic nanoparticles' surfaces. The sugar ligands' UV region was used to analyze lambda max (λ_{max}) and the full-width-half-maxima (λ_{fwhm}), which were determined as described in the literature [36], to understand how these two affected the monitored interactions. In 210–350 nm region, LMA ligand gave two peaks at 238 and 300 nm, and similarly LMA_Arg_AgNP, LMA_Arg2_AgNP and LMA_Arg_Cl_AgNP gave the peaks at 236/297 nm, 237/300 nm and 238/300 nm, respectively. However, LMA_AgNP1 and LMA_AgNP2 did not give any peak at 216–265 nm range while both gave distorted peaks at 304 nm. Besides, LMA_AgNP1 gave a slight peak at 243 nm, which disappeared in the case of higher silver ion concentration (LMA_AgNP2). In contrast to these, a new absorption arose between 260 and 290 nm, where 274 nm peak was observed for LMA_AgNP1 and LMA_AgNP2, which was not present in the sugar ligand and rest of the AgNPs. The λ_{fwhm} for 216–265 nm range and 270–340 nm ranges were 21/25 nm, 8/26 nm, 12/23 nm and 13/26 nm for LMA ligand, LMA_Arg_AgNP, LMA_Arg2_AgNP, LMA_Arg_Cl_AgNP, respectively. Upon AgNP SPR peak formation in LMA_Arg_AgNPs and LMA_Arg2_AgNPs in UV-Vis spectra, sugar ligand/AgNP peak ratio showed continuous decrease. All these showed that Arginine has higher affinity for Ag^+ ions, but LMA gradually reduced Ag^+ ions into AgNP. The UV-Vis spectra shows that LMA_Arg_AgNP gave SPR peak within 5-min incubation while presence of SPR peak in LMA_Arg2_AgNP within 3 h incubation. LMA_AgNP1 gave LMA_AgNP2 two SPR peaks at 572 and 724 nm while the SPR peaks at 550 nm and 516 nm were observed in LMA_Arg_AgNP and LMA_Arg2_AgNP, respectively. It is clear that Arginine did not only alter the reaction kinetic, but also it posed effect on the morphology (SPR pattern gives information about the morphology and size of the AgNPs [37]), which is expected since Arginine has very strong affinity for Ag^+ ion and can interact with silver nanoparticles through amino groups [38,39]. However, from these experiments we cannot conclude that whether Arginine joined the nanoparticle formation or not within the first minutes or hours depending on the sugar ligands. In the case of LMA_Arg_Cl_AgNP spectra, a slight peak formation started between 500 and 650 nm range in 5 h incubation period.

The UV-Vis peak at 203 nm in G5AS ligand spectrum was observed in the spectra of G5AS_Cl_AgNPs and G5AS_Arg_Cl_AgNPs while 201 and 205 nm peaks were observed in G5AS_AgNP2 spectrum. G5AS ligand, also, gave λ_{max} at 300 nm (λ_{fwhm} 23 nm) and a shoulder-like peak at 344 nm while G5AS_AgNP and G5AS_AgNP2 gave λ_{max} at 295 nm (λ_{fwhm} 32 nm) but no shoulder-like peak was observed. Similarly, λ_{max} at 295 nm was observed for G5AS_Cl_AgNPs. G5AS_Arg_AgNPs, G5AS_Arg2_AgNPs and G5AS_Arg_Cl_AgNP gave λ_{max} at 290 (λ_{fwhm} 20 nm) and 391 nm (λ_{fwhm} 50 nm), 282 and 337 nm, 285 and 336 nm (λ_{fwhm} 31 nm), respectively (Fig. 3). In the 450–900 nm range, G5AS_AgNP1, G5AS_AgNP2 and G5AS_Arg_AgNP gave λ_{max} at 526 nm, and among these G5AS_Arg_AgNP gave the strongest peak. In contrast to this, the other formulations did not give any peak. Lacking characteristic SPR peaks clearly show that formation of metallic Ag particles was suppressed by the presence of excess Arginine.

LSA mediated AgNP and Ag/AgCl_NP synthesis showed very slow kinetic. In contrast to LSA_AgNPs, LSA_Arg_AgNP and Arg_AgNP, LSA-Arg_AgCl_NPs and Arg_AgCl_NP nanoparticle formations were faster, which were seen within 3-h incubation. LSA ligand gave λ_{max} at 260 nm, which did not alter upon AgNP or AgCl formation with/without Arginine presence. However, in 200–220 nm region, absorption enhancements and peak formations were observed upon introduction of silver ions. Similar observations were observed for LPSA synthesized AgNPs, and alterations in response to differentiations in the formulations sugar moieties within the LPSA ligands were clear while no clear alterations in the aromatic group were observed. It is known that sulfonyl groups can strongly interact with Ag^+ ion [29,40], so formation of solid LSA_AgNPs or LPSA_AgNPs did not happen under the experimental conditions. Besides, this strong interaction might be another reason for the no alterations observed for the phenyl ring related UV-Vis absorption.

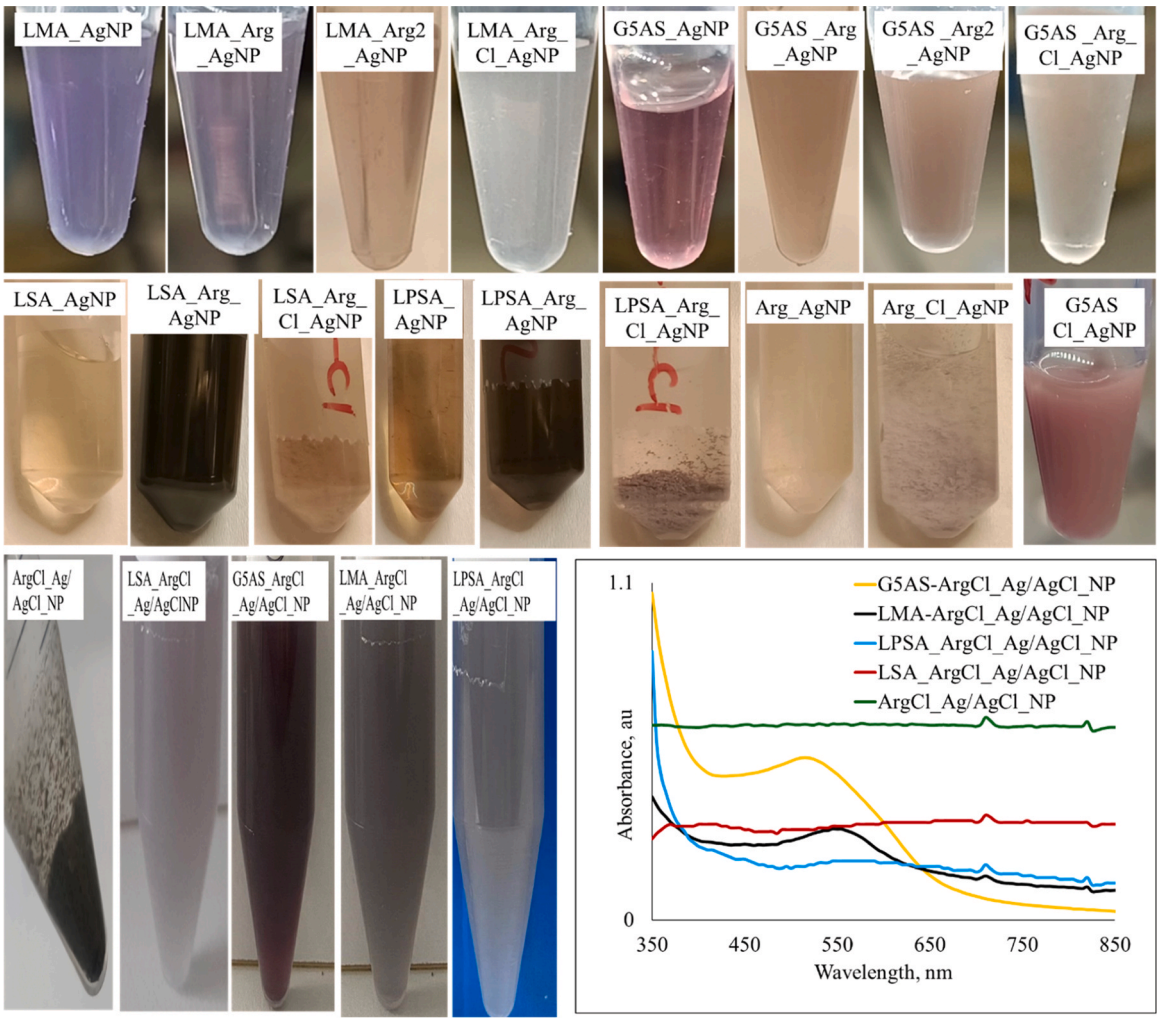

Fig. 2. Digital camera images of the nanoparticle formulations and UV-Vis of sugar ligand synthesized ArgCl_Ag/AgCl_NPs.

3.2. Infrared spectroscopic characterization of Ag/AgCl_NPs

The major IR assignments of L-Arginine are -NH stretching (3359 and 3296 cm^{-1}), -OH stretching (3051 cm^{-1}), -CH and -CH_2 stretching (2944 and 2862 cm^{-1}), stretching C═O (1719 cm^{-1}), stretching C═N of $CN_3H_5^+$ (1674 cm^{-1}), and ν_{as} COO^- and δNH_2 (1614 cm^{-1}), C═O stretching and NH_2 scissoring (1552 cm^{-1}), asymmetric stretching C-H (1473 cm^{-1}), ν_s COO^- bending -CH_2 (1419 cm^{-1}), δC-H (1375 cm^{-1}), bending -OH (1331 cm^{-1}), CCC stretching + stretching rNH_3^+ of side group (1182 cm^{-1}), νC-N and rocking C-NH_3^+ (1133 cm^{-1}), C-N vibration and bending -OH (975 cm^{-1}), γNH_2 and rCH_2 or just rCH_2 (766 and 699 cm^{-1}) [41–44]. IR spectrum of L-Arginine gets altered upon its interaction with silver nanoparticles, and most of the peaks get lost [20]. The IR spectra of the Arg_AgNP, Arg_Cl_AgNP1 and Arg_Cl_AgNP2 gave stretching -OH of COOH band at 3417 ± 10 cm^{-1} [20] while stretching of amine group was not present within 3100–3400 cm^{-1} range. The wavenumbers at 1631 ± 1 cm^{-1} and 1382 ± 1 cm^{-1} correspond to bending NH_2 and symmetric stretching COO^-, respectively. The peaks at 1562 cm^{-1} correspond to asymmetric COO^- stretching and only found in Arg_AgNP while the weak peak at 1174 cm^{-1} reveals the presence of CCC stretching + stretching C-N (or rocking NH_3^+ of side group) and only found in Arg_AgNP and Arg_Cl_AgNP1. All these show that the introduction of chloride ion suppresses the presence of stretching C-N (or rocking NH_3^+ of side group) and its further increase eliminates the IR band of COO^- asymmetric stretching.

IR spectra of the nanoparticle formulations revealed that introduction of L-Arginine Hydrochloride or L-Arginine into the sugar ligand-Ag^+ ion reaction media posed strong effect on the surface chemistry of the Ag/AgCl_NPs. This effect was also valid for the interactions that took place between L-Arginine and Ag/AgCl_NPs. Table 1 lists the IR peaks for G5AS_ArgCl_Ag/AgCl_NPs, LMA_ArgCl_Ag/AgCl_NPs, LPSA_ArgCl_Ag/AgCl_NPs and LSA_ArgCl_Ag/AgCl_NPs while Fig. 4 shows IR spectra of all the formulations. The presence of L-Arginine specific IR bands became visible upon sugar ligand introduction to the Ag/AgCl_NP synthesis medium. LSA_AgNP IR spectrum only gave peaks at 3372 cm^{-1} (OH of sugars), 1625 cm^{-1} (NH), 1604 cm^{-1} (ArC═N), 1498 cm^{-1} (aromatic ring), 1347 cm^{-1} ω(CH_2), 1166 cm^{-1} (ArC-N-C), 1124 cm^{-1} (SO_2 stretching), 1078 cm^{-1} (S-OH), 1032 (OH of sugars) and 822 cm^{-1} (aromatic ring + sugar residue related vibrations) (Fig. 4**c**) while LPSA_AgNPs gave peaks at 3357 cm^{-1} (OH of sugars), 2923 (C-H stretching), 1628 cm^{-1}(NH), 1598 cm^{-1} (ArC═N), weak 1516 cm^{-1} (aromatic ring), 1384 cm^{-1}, 1358 cm^{-1} ω(CH_2), 1143 cm^{-1} (NH), 1066 cm^{-1} (vibrations from S-O + C-N), 1044 cm^{-1} (OH of sugars), weak 887 cm^{-1} and 822 cm^{-1} (sugar residue and phenyl ring vibrations) [45]. Upon L-Arginine introduction, clear representation of the amine groups was observed throughout the IR spectra of the corresponding nanoparticles while the IR spectrum of Arg_AgNPs only showed the bending vibration of NH_2 as discussed above. The IR spectrum of LPSA_Arg_AgNP gave quite similar IR peaks obtained for LPSA_ArgCl_Ag/AgNPs while carboxyl group bands were not clear in LPSA_Arg_Cl_Ag/AgCl_NPs. Similar observations were obtained for LSA, G5AS and LMA synthesized Ag/AgCl_NPs using different formulations.

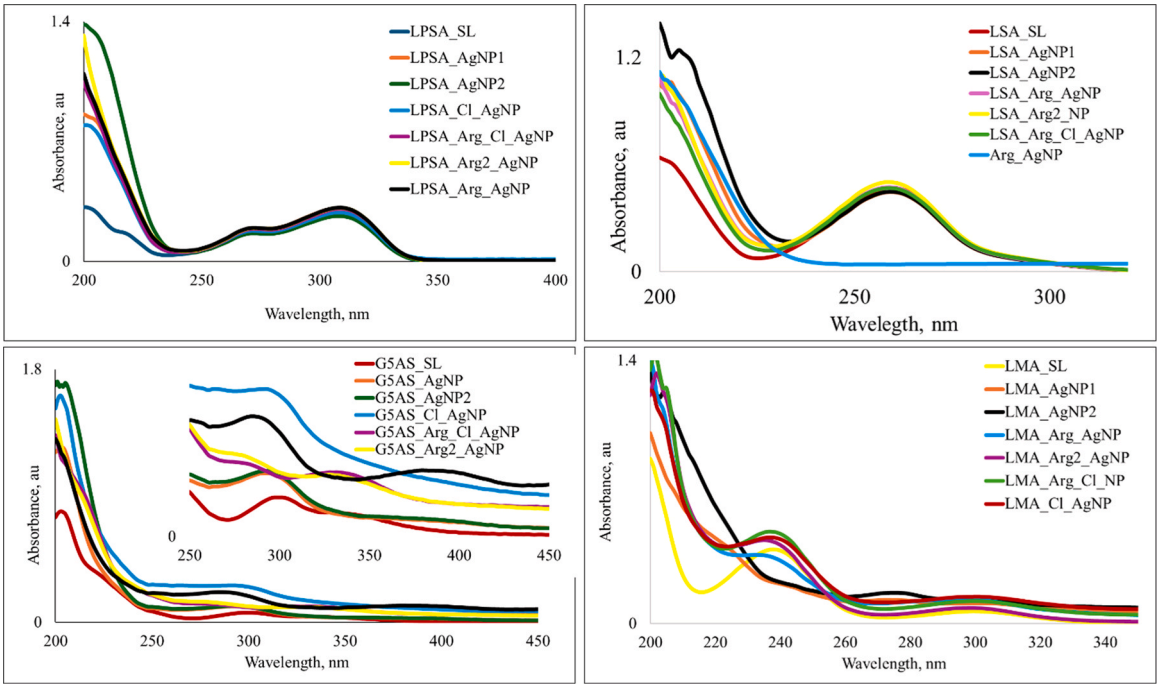

Fig. 3. UV-Vis spectra of sugar ligands and nanoparticle formulations.

Table 1
IR assignments of Ag/AgCl_NPs.

G5AS_ArgCl_Ag/AgCl_NPs
ν(OH) 3300 cm^{-1}; ν(CH) 2932 cm^{-1}; ν(C═N) 1666 cm^{-1}; ν(C═O) 1624 cm^{-1}; δ(CO_2^-) + δ(N-H) 1585 cm^{-1}; δ(NH_3^+) 1513 cm^{-1}; CH_2 scissoring 1453 cm^{-1}; $\nu_s(CO_2^-)$ 1397 cm^{-1}; ν(ArC-N) 1325 cm^{-1}; δ(NH) + τ(CH_2) + δ(C-OH of CO_2^-) 1209 cm^{-1}; ρ(NH_3^+) 1127 cm^{-1}; ν(C-O) 1072 cm^{-1}; ν(OH of sugar residue) 1033 cm^{-1}; ν(CC) + ν(CO) + β(CCH) 901 cm^{-1}; ω(NH) + τ(NH) 850 cm^{-1}; δ(CO_2^-) + ν(C=CH) 822 cm^{-1}; δ(C-H) 785 cm^{-1}; ν(CH_2) 747 cm^{-1}; aromatic ring vibrations 695 cm^{-1}; ν(-O-AgNP) 662 cm^{-1}; ω(CO_2^-) 641 cm^{-1}
LSA_ArgCl_Ag/AgCl_NPs
ν(OH) 3309 and 3040 cm^{-1}; $\nu_s(NH_2)$ 3177 cm^{-1}; ν(CH) + ν(CH_2) 2961 and 2925 cm^{-1}; ν_{as}(C═N) 1664 cm^{-1}; δ(NH_3^+) + $\delta_{as}(CO_2^-)$ 1631 cm^{-1}; ν(ArC=C) + ν(ArH-C-H) + ν(SO_2) + δs (NH_3^+) 1518 cm^{-1}; ν(ArC=C) 1452 cm^{-1}; $\nu_s(CO_2^-)$ 1395; ω(CH_2) 1355 cm^{-1}; ν_s(C═O) 1318 cm^{-1}; δ(OH of CO_2^-) 1211 cm^{-1}; ν_{as}(C-N-C) 1154 cm^{-1}; r(NH_3^+) + $v_s(SO_2)$ 1125 cm^{-1}; ν(S-OH) + ν(C-N) + ω(NH_2) 1066 cm^{-1}; ν(OH of sugars) 1026 cm^{-1}; ω(NH_2) 865 cm^{-1}
LPSA_ArgCl_Ag/AgCl_NPs
ν(OH) 3325, 3174, 3048 and 3071 cm^{-1}; ν(CH) 2928 cm^{-1}; ν(C═N) 1672 cm^{-1}; $\nu_{as}(CO_2^-)$ + δ(NH_2) 1630 cm^{-1}; ν(ArC=C) + ν(C═O) 1592 cm^{-1}; δ(NH) + δ(NH_3^+) 1516 cm^{-1}; CH_2 scissoring 1452 cm^{-1}; $\nu_s(CO_2^-)$ 1399 cm^{-1}; δ(CH_2) + ν(CC) 1327 cm^{-1}; δ(OH of CO_2^-) 1211 cm^{-1}; r(NH_3^+) 1131 cm^{-1}; ν(C-N) 1103 cm^{-1}; ν(S-O) + ν(C-N) 1070 cm^{-1}; ν(OH of sugars) 1041 cm^{-1}; ω(NH) + t(NH) 848 cm^{-1}; ν(CC) + β(CCH) + (O-C-O) 824 cm^{-1}; r(CH_2) 749 cm^{-1}
LMA_ArgCl_Ag/AgCl_NPs
ν(OH) 3286 and 3058 cm^{-1}; $\nu_s(NH_2)$ 3156 cm^{-1}; ν(CH) and ν(CH_2) 2957 and 2931 cm^{-1}; ν_{as}(C═N) 1671 cm^{-1}; δ(NH_3^+) + $\delta_{as}(CO_2^-)$ 1621 cm^{-1}; 1511 cm^{-1}; ν(ArC=C) 1453 cm^{-1}; $\nu_s(CO_2^-)$ 1399 and 1325 cm^{-1}; δ(OH of CO_2^-) 1208 cm^{-1}; ν_s(C═O) cm^{-1}; C-N stretching1161 cm^{-1}; ν_{as}(C-N-C) 1120 cm^{-1}; ν(S-OH) + ν(C-N) + ω(NH_2) 1079 cm^{-1}; ν(OH of sugars) 1025 cm^{-1}; ν(CC) + ν(CO) + β(CCH) 894 cm^{-1}; ω(NH_2) 846 cm^{-1}; 821 cm^{-1}; δ(C-H) 790 cm^{-1}; r(CH_2) 750 cm^{-1}

Arginine interaction with silver nanostructures (e.g. nanoclusters) take place through side-chain nitrogen groups and -OH of COOH group [46]. Besides, the interaction between L-Arginine and Ag^+ ion happen through side and α-amine group and carboxyl group while the shortest bond (highest affinity) was from the side amine group [38]. So, lack of amine group representation at 3000–3300 cm^{-1} region in Arg_AgNPs is not related to the merge of -OH and -NH_2 as suggested in the literature [20], rather it can be resulted from the strong adsorption of -OH group on the AgNPs surface since the functional groups interacting with metal surface (such as nanoparticles' surfaces) give enhanced IR bands [47]. So, it is possible to speculate that the strong -OH adsorption suppressed the presence of amine group related bands in AgNPs. It is also known that IR bands give shifts (mostly red shift) upon adsorption on the nanostructure surfaces [46,48]. The differences among the Ag/AgCl_NPs IR spectra in response to the co-administration of the sugar ligands with Arginine can be a strong sign that primary and side-chain amine groups in Arginine both joined the stabilization of Ag/AgCl_NPs, which then affected how the sugar ligands interacted with the nanoparticles. Besides, alterations in carboxylic group IR bands also revealed that the carboxylic group of Arginine showed itself in LPSA_ArgCl_Ag/AgCl_NPs, LSA_ArgCl_Ag/AgCl_NPs and LMA_ArgCl_Ag/AgCl_NPs while that was not very clear in G5AS_ArgCl_Ag/AgCl_NPs since G5AS has carboxylic group.

3.3. *Morphological and crystallographic characterization of the Ag/AgCl_NPs*

Fig. 5 shows that LMA-ArgCl_Ag/AgCl_NPs exist as leaf-like nanoparticles, spherical and anisotropic nanoparticles. The size of the leaf-like nanoparticles is in the micron range, while about 90 % of the spherical nanoparticles are between 3 and 5.5 nm in size, and the anisotropic nanoparticles have cross-sections of ~16 × 52 nm (Fig. 5**B**). The presence face centric cubic crystal of metallic AgNPs was revealed by 38.14° (111), 44.56 ° (200), 64.52° (220) and 77.55° (311) 2θ angles [49,50]. The presence of the 2θ peaks 27.51°, 32.15°, 46.04°, 54.60°, 57.49°, 67.47°, 74.41° and 76.57° corresponding to (111), (200), (220), (311), (222), (400), (331) and (420) miller indices, respectively, revealing the presence of face centric AgCl nanocrystals [4,6,51] (Fig. 5**F**). The tiny peak at 50.25 ° and the joint peaks at 67.59° and 76.85 ° can be assigned to (104), (112) and (201) *4 H hcp* AgNPs,

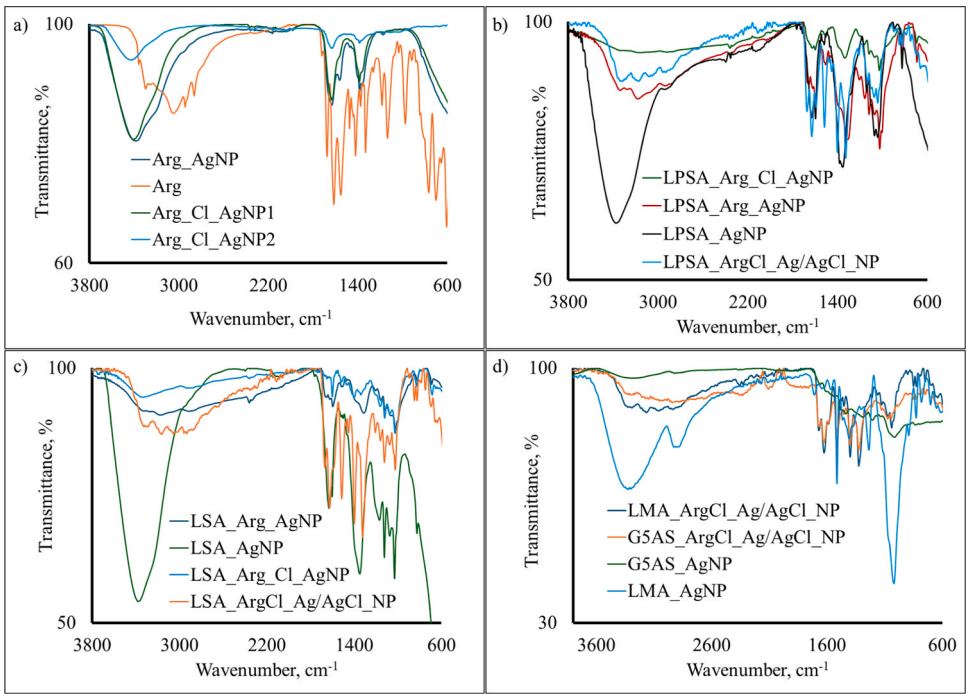

Fig. 4. IR spectra of the nanoparticle formulations synthesized in the presence of Arginine alone (a), LPSA sugar ligand (b), LSA sugar ligand (c) and LMA and G5AS sugar ligands (d).

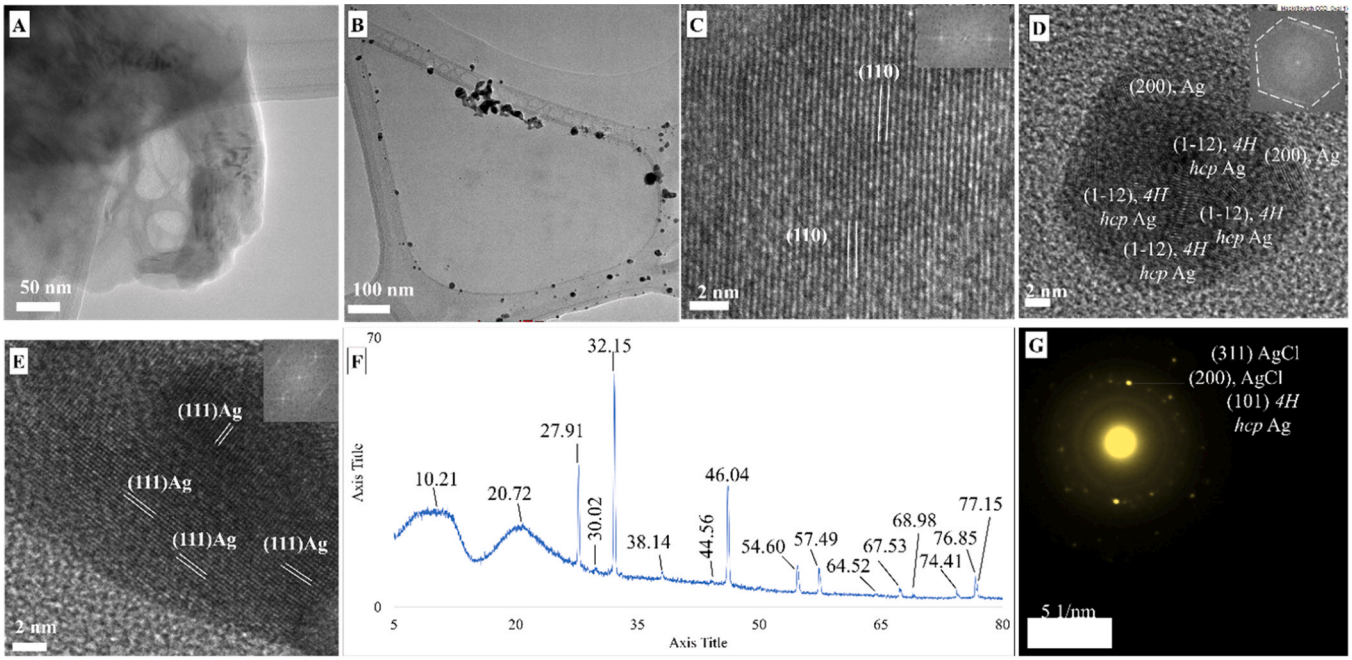

Fig. 5. TEM micrographs, SAED and XRD spectra of LMA-ArgCl_Ag/AgCl_NPs.

respectively. The interplanar spacing of film-like AgNP was obtained as 0.326 nm (Fig. 5**C**) that was assigned to 2θ 27.91° of *fcc* AgCl NPs. Fig. 5**E** shows that the d_{sp} 0.234 mm belongs to *fcc* metallic AgNPs' (111) miller indices. However, Fig. 5**D** reveals presence of (200) *fcc* and (1−12) *4 H hcp* AgNP faces. It is possible that metallic AgNPs and Ag/AgCl_NPs were formed independent from each other. SAED pattern reveals (200) AgCl with 0.283 nm interplanar spacing [52], Since XRD reveals the crystalline structure of the bulk samples, it is expected to see metallic AgNPs and AgCl NPs 2Θ angles together (Fig. 5**F**).

The film-like structure of G5AS-ArgCl_Ag/AgCl_NPs (Fig. 6**-A/-B**) gave 0.33 nm *d* spacing that can reveal the presence of (111) miller indices of AgCl nanoparticles (Fig. 6**-C/-D**). AgNPs can form within AgCl crystals [14], and their co-existence have been reported [12], and SPR band seen in Fig. 2 proves this even though the miller indices only reveal the presence of AgCl_NPs. The literature shows similar results as miller indices belong to metallic AgNPs and AgCl_NPs appear in the XRD spectrum [5]. The EDX spectrum (Fig. 6**E**) shows the presence of silver and chloride, and the inserted table reveals chloride/silver atomic ratio is ~6, which was ~4 in LMA-ArgCl_Ag/AgCl_NPs (data was not shown). It is also known that AgCl nanoparticles can form large particles since

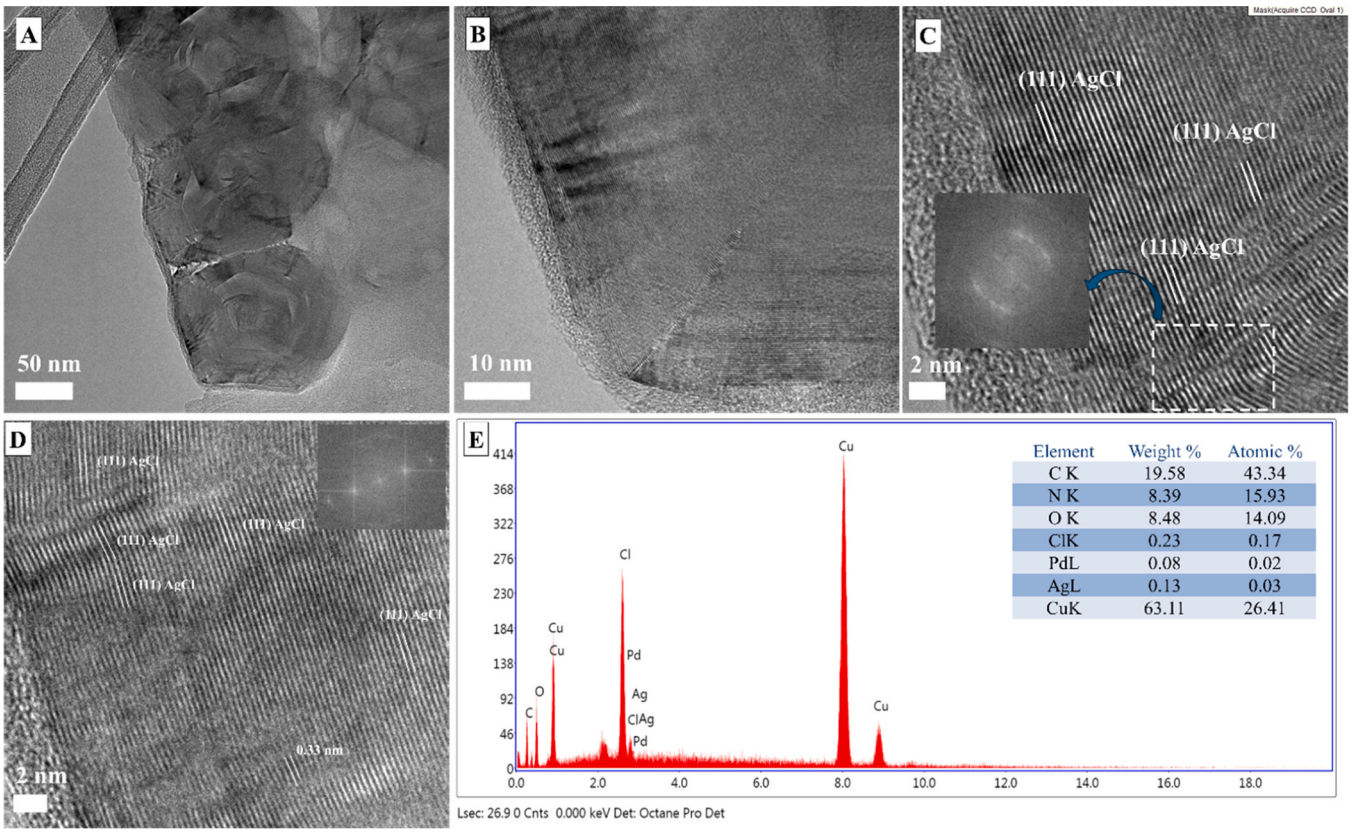

Fig. 6. TEM micrographs of G5AS-ArgCl_Ag/AgCl_NPs.

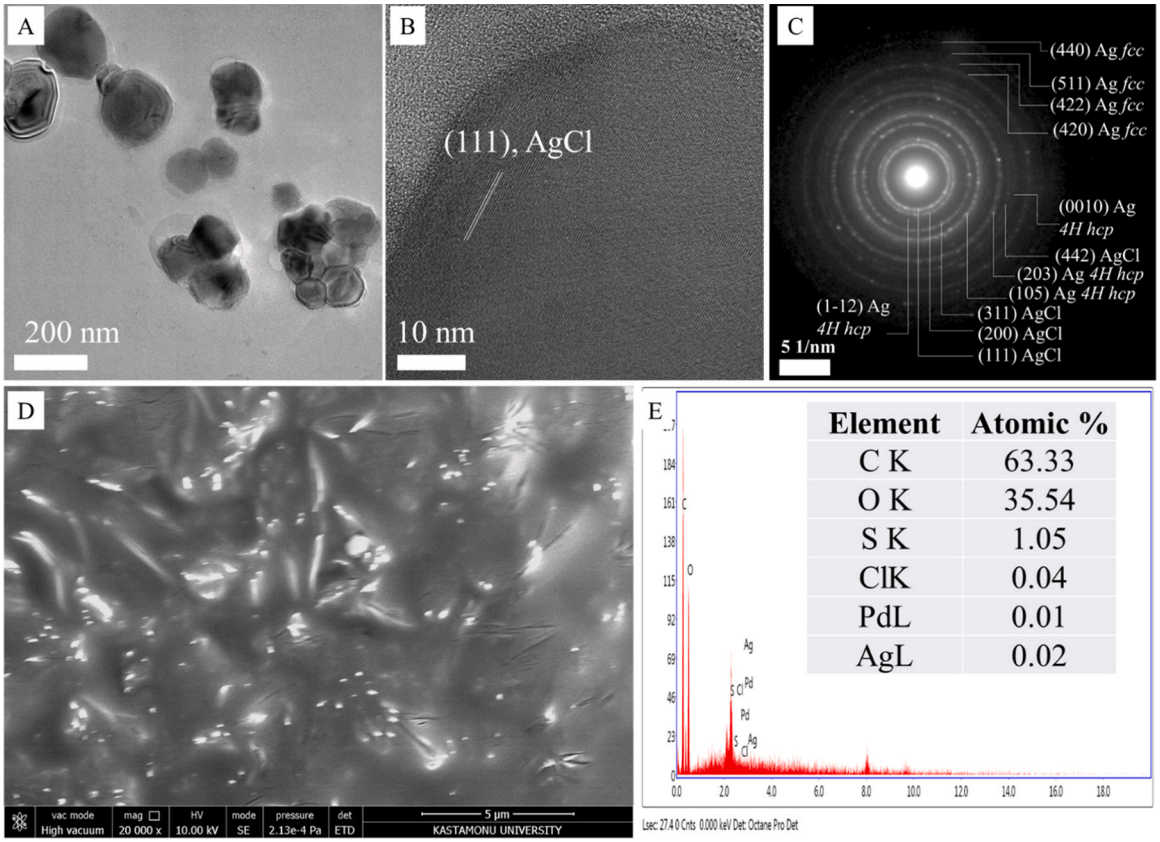

Fig. 7. LPSA-ArgCl_Ag/AgCl_NPs HRTEM-SAED and SEM-images, and EDX spectrum.

Ag^+ and Cl^- can interact with six atoms [53], so larger forms were expected. The presence of lead in EDX spectra of the samples is related to the lead-coated copper tape, on which samples were placed for SEM-EDX analysis. Hereby, it is also critical to point out that presence of copper in G5AS-ArgCl_Ag/AgCl_NPs and LMA-ArgCl_Ag/AgCl_NPs EDX spectra reveal the Ag/AgCl_NP film structure was not very tight or dense in comparison to the Ag/AgCl_NP films synthesized with LPSA and LSA ligands (their EDX spectra did not give copper EDX pattern).

Fig. 7**A** shows anisotropic ~75–195 nm sized particles while Fig. 7**D** reveals presence of film-like structure and scattered particles with 120–220 nm sized particles. The SAED pattern of AgNPs gave *4 H hcp* phases with (1−12), (105), (203) and (0010) miller indices in addition to *fcc* phases with (420), (422), (511) and (440) miller indices [54]. The presence of AgCl was revealed by (111), (200), (311) and (422) *fcc* AgCl crystals (Fig. 7**C**). Besides, it is noteworthy to mention that some of the miller indices from AgCl_NPs and Ag_NPs could give one peak. Fig. 7**B** reveals presence of crystal infringement with (111) of AgCls ($d_{spacing}$ ~0.34 nm). The inserted table within EDX spectrum (Fig. 7**E**) showed chloride/silver ratio was 2, which was different that G5AS_ArgCl_Ag/AgCl_NPs. UV-Vis studies showed that the interactions of silver ions with LPSA and G5AS were distinctly different from each other. It is possible that this situation affected the interaction between chloride ion and silver ion in the media, so based on the EDX results it can be speculated that coordination or ionic interaction between the sugar ligand and silver or silver nanoparticles showed dependence on the sugar ligand chemistry. It is also important that LPSA- and LSA-synthesized ArgCl_Ag/AgCl_NPs showed distinctly different morphology and size, which is also a sign that sugar ligand chemistry played a critical role for the interactions that took place in the reaction medium.

Fig. 8**A** shows the nanoparticles are anisotropic with 26–91 nm size range, which mostly fall into 50 ± 10 nm range. HRTEM images showed some of the nanoparticles have (111) *fcc* AgNP with 0.235 nm crystal infringement and (111) AgCl with 0.34 nm crystal infringement (Fig. 8**B**). This might not reflect the formation of individual AgNPs and AgCl_NPs, rather it could be related to formation of different phases during the nanoparticle formation. The SAED image reveals the nanoparticles are composed of metallic AgNPs with (111) *fcc* and (102) 4 H *hcp* miller indices and AgCl_NPs with (111), (400) and (441) miller indices. The $d_{spacing}$ 0.12 nm could be assigned to (441) *fcc* AgCl or (202) 4 H *hcp* AgNPs (Fig. 8**C**). SEM-EDX gave presence of Ag, but percentage presence was given as 0, which was not assigned to any known phenomenon (data not shown).

The illustrative XRD and SAED studies showed that synthesis of ArgCl_Ag/AgCl_NPs were successful. It is noteworthy to mention that coexistence of metastable *4 H* hexagonally close packed AgNPs in *face centric cubic* AgNP crystals have been reported in the literature [31,55]. Crystal reformation and/or phase-interaction can show dependence on the drying process of the suspended AgNPs, so SAED and XRD patterns can give such differences [55]. Besides, *4 H hcp* phases can extend upon interaction with *fcc* phases [55] even though the irreversible *4 H* phase transition to *fcc* phase can promote enlargement of *fcc* nanoparticle grain size [56]. Therefore, the presence of *4 H hcp* phases are not an abnormal observation.

3.4. Antibacterial characterizations of the Ag/AgCl_NPs

Fig. 9**-B/-C** show that LPSA_ArgCl_Ag/AgCl_NPs and LSA_ArgCl_Ag/AgCl_NPs gave 1.8375 μM MIC and MBC value for the tested Colistin and carbapenem resistant *E. coli* species while G5AS_ArgCl_Ag/AgCl_NPs and LMA_ArgCl_Ag/AgCl_NPs gave 3.675 and 7.35 μM MIC and MBC value for the two *E. coli* species. According to our pre-test results, the LPSA and LSA synthesized formulations gave better antibacterial activity compared to free Ag^+ ions ($AgNO_3$: 5 μM MBC under the tested conditions), which can be related to sulfonyl group's interactions with Ag^+ ions make them less affected by the proteins in the culture media. It is also important to note that Arginine can alter cell surface physicochemical properties of gram (-) bacterial species [57]. Besides, AgCl nanoparticles can also advance the antibacterial activity of classical antibiotics when they are combined [58]. It is also critical to mention that synergistic action of Ag/AgCl_NPs dependent on the antibiotic chemistry [5]. Nanoparticles may not show their toxicities at higher concentrations while their lower concentrations can pose higher antibacterial activity when they are used at relatively lower concentrations [26], so it is understandable that LSA_ArgCl_Ag/AgCl_NPs showed lower toxicities at its highest tested concentrations. According to the European Committee on Antimicrobial Susceptibility Testing, > 1 μg/mL MIC values refer to resistant species for the tested antibiotic [59]. So, we tested the higher concentrations, and 100 and 10 μg/mL Colistin to show the resistance of the used *E. coli* species. Although the nanoparticles did not give nanogram/mL MIC/MBC values, the nanoparticles gave relatively low MIC/MBC values for the resistant *E. coli* species. Besides, biofilm formation (Fig. 9A) was present for *E. coli* species −1/-2 for the control and Colistin treatment did not prevent biofilm formation for *E. coli* species 1 while the treatment at 100 μg/mL concentration prevented the biofilm growth for *E. coli* species 2. LPSA_ArgCl_Ag/AgCl_NPs at 1.8375 μM, LSA_ArgCl_Ag/AgCl_NPs at 29.4 μM and LMA_ArgCl_Ag/AgCl_NPs at 1.8375 μM concentrations did not prevent biofilm growth for *E. coli* species 1 while the nanoparticles prevented the biofilm growth at all the tested concentrations. From the results, it can be speculated that the nanoparticles are not just effective in killing the Colistin resistant bacterial species, but also they can prevent biofilm growth, which is an important virulence factor [60]. Besides, studies revealed that Ag/AgCl_NPs can show better antibacterial activity compared to silver nanoparticles as well [61].

The main limitations of the study can be listed as (i) the exact ratio of Ag^0 content within Ag/AgCl_NPs were not characterized and calculated. (ii) Surface charge can be critical for nanoparticles' colloidal stability, so a contemplated study should be done whether there was a direct relationship between the stability and surface for the particles. The other prominent limitation (iii) is that Argine content was not checked using

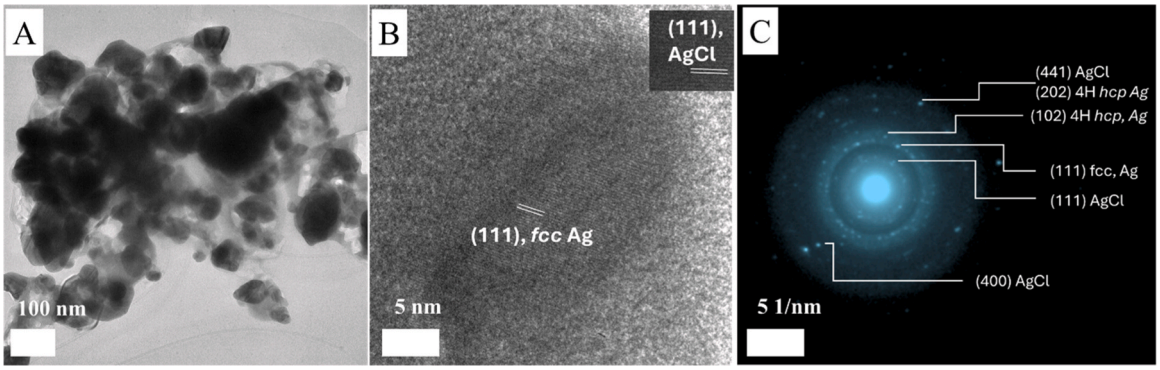

Fig. 8. TEM and SAED images of LSA_ArgCl_Ag/AgCl_NPs.

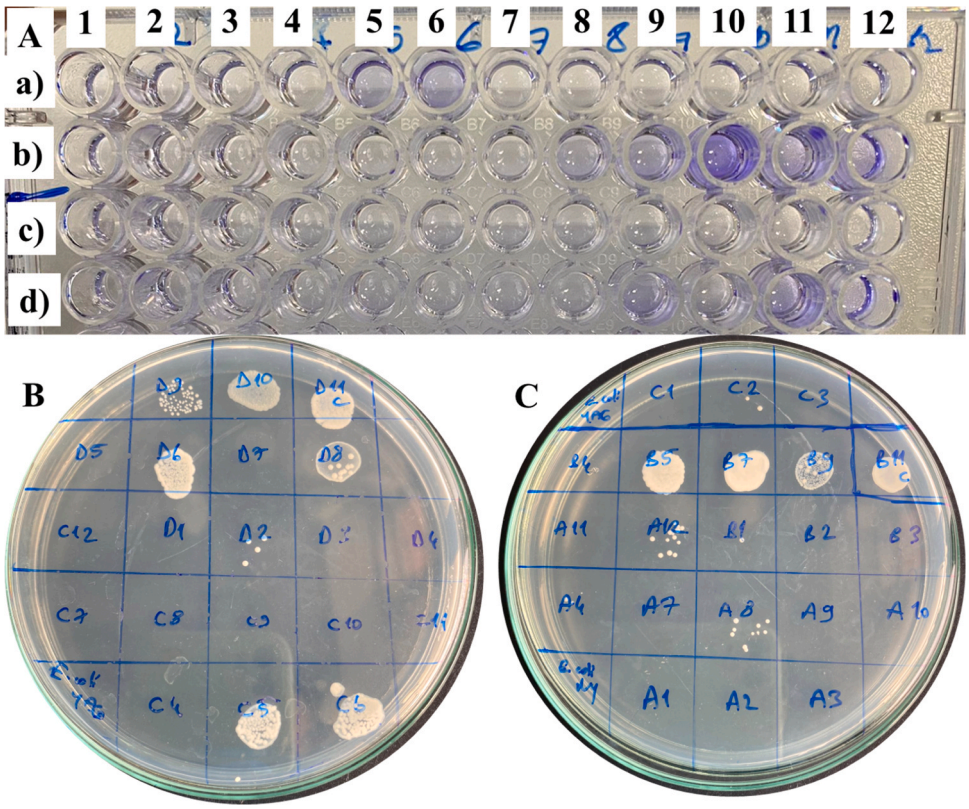

Fig. 9. Biofilm (A) and minimum bactericidal characteristics of (B/C) of the nanoparticles. Antibacterial characteristics of the ArgCl_Ag/AgCl_NPs. a1–5/c1–5: LPSA_ArgCl_Ag/AgCl_NP; a6–10/c6–10: LSA_ArgCl_Ag/AgCl_NP; a11-b3/c11-d3: G5AS_ArgCl_Ag/AgCl_NP; b4–8/d4–8: LMA_ArgCl_Ag/AgCl_NP; b9–10/d9–10: Colistin (100 and 10 μg/mL, respectively), and b11–12/d11–12: Control. ArgCl_Ag/AgCl_NP concentration range was 29.4–1.8375 μM. a/b: *E. coli* species 1 and c/d: *E. coli* species 2.

thermogravimetric analysis, which could help to explain how different Arginine content affected the IR presence of key functional groups coming from the sugar ligands and Arginine. Finally (iv), a detailed X-ray photoelectron spectroscopy is needed to understand the conversion rate of Ag^{+} into Ag^{0} depending on the concentrations and chemistry of the compounds.

4. Conclusion

Hereby, we showed that the morphology and size of the ArgCl_Ag/AgCl_NPs were strongly influenced by the sugar ligand chemistry. Galactose 5-aminosalisylic acid and Lactose 4-methoxyaniline ligands caused sheet-like ArgCl_Ag/AgCl_NPs while Lactose sulfanilic acid and Lactose 4,4'-aminofenilsulfone ligands caused anisotropic ArgCl_Ag/AgCl_NPs and film-like structure formations. The presence of Arginine in the synthesis media affected the sugar ligands' interaction with silver ions, thus influencing the ArgCl_Ag/AgCl_NP formation kinetic and surface chemistry. IR studies revealed that Arginine interacted with AgNPs and ArgCl_Ag/AgCl_NPs mainly through carboxylic and guanidino groups while introduction of the sugar ligands also forced Arginine's primary amine group to interact with the formed nanoparticles. The nanoparticle formulations showed strong antibacterial activities for the Colistin resistant *E. coli* species, where LPSA and LSA synthesized formulations gave better performance in comparison to the G5AS and LMA synthesized ones. It is also noteworthy to mention that the ArgCl_Ag/AgCl_NPs can be used as coating material since they tend to form film-like structures.

CRediT authorship contribution statement

Şuheda Bolat- Carried out major experiments including characterization, written original draft. Suna Değirmenci- Carried out experiments and characterization. Abdurrahman Gümüş- Carried out characterizations. Zafer Sancak- Supervision, project administration, reviewing and editing the final draft of the work. İdris Yazgan-Conceptualization of the nano synthesis part, data analysis, reviewed and edited original draft, and communication of the work to the journal.

Declaration of Competing Interest

The authors declare that they have no known competing financial interests or personal relationships that could have appeared to influence the work reported in this paper.

Acknowledgement

This study was supported by Kastamonu University Internal Fundings (Grant number KÜ-BAP01/2021–25).

References

[1] Y. Kashid, S. Ghotekar, M. Bilal, S. Pansambal, R. Oza, R.S. Varma, V.H. Nguyen, H. C. Ananda Murthy, D. Mane, Bio-inspired sustainable synthesis of silver chloride nanoparticles and their prominent applications, J. Indian Chem. Soc. 99 (2022) 100335, https://doi.org/10.1016/j.jics.2021.100335.

[2] M.P. Patil, L.L.A. Piad, E. Bayaraa, P. Subedi, N.H. Tarte, G.Do Kim, Doxycycline hyclate mediated silver–silver chloride nanoparticles and their antibacterial activity, J. Nanostruct. Chem. 9 (2019) 53–60, https://doi.org/10.1007/s40097-019-0297-6.

[3] N.D. Trinh, T.T.B. Nguyen, T.H. Nguyen, Preparation and characterization of silver chloride nanoparticles as an antibacterial agent, Adv. Nat. Sci. Nanosci. Nanotechnol. 6 (2015) 045011, https://doi.org/10.1134/S1560090417060082.

[4] Z. Hachem, R. Kashmar, A.M. Abdallah, R. Awad, M.I. Khalil, Characterization, antioxidant, antibacterial, and antibiofilm properties of biosynthesized Ag/AgCl nanoparticles using Origanum ehrenbergii Boiss, Results Mater. 21 (2024) 100550, https://doi.org/10.1016/j.rinma.2024.100550.

[5] I. Ghiuta, C. Croitoru, J. Kost, R. Wenkert, D. Munteanu, Bacteria-mediated synthesis of silver and silver chloride nanoparticles and their antimicrobial activity, Appl. Sci. 11 (2021) 3134, https://doi.org/10.3390/app11073134.

[6] J.N. Araújo, A. Tofanello, V.M. da Silva, J.A.P. Sato, F.M. Squina, I.L. Nantes, W. Garcia, Photobiosynthesis of stable and functional silver/silver chloride nanoparticles with hydrolytic activity using hyperthermophilic β-glucosidases with industrial potential, Int. J. Biol. Macromol. 102 (2017) 84–91, https://doi.org/10.1016/j.ijbiomac.2017.04.001.

[7] T. Tsuji, Y. Okazaki, T. Higuchi, M. Tsuji, Laser-induced morphology changes of silver colloids prepared by laser ablation in water. Enhancement of anisotropic shape conversions by chloride ions, J. Photochem. Photobiol. A Chem. 183 (2006) 297–303, https://doi.org/10.1016/j.jphotochem.2006.05.021.

[8] J. Luis, T. López, S. Lázaro, M. Susana, D. Rosa, M.A. Alvarez, L. Abraham, G. Rivera, R. López, G. Carlos, E. Lobato, Medicinal plants extract for the bio-assisted synthesis of Ag/AgCl nanoparticles with antibacterial activity, J. Clust. Sci. 36 (2025) 20, https://doi.org/10.1007/s10876-024-02722-w.

[9] P. Wang, B. Huang, Z. Lou, X. Zhang, X. Qin, Y. Dai, Z. Zheng, X. Wang, Synthesis of highly efficient Ag@AgCl plasmonic photocatalysts with various structures, Chem. - A Eur. J. 16 (2010) 538–544, https://doi.org/10.1002/chem.200901954.

[10] J. Bai, Y. Li, M. Li, S. Wang, C. Zhang, Q. Yang, Electrospinning method for the preparation of silver chloride nanoparticles in PVP nanofiber, Appl. Surf. Sci. 254 (2008) 4520–4523, https://doi.org/10.1016/j.apsusc.2008.01.051.

[11] S.P. Pasaribu, M. Ginting, I. Masmur, J. Kaban, Hestina, Silver chloride nanoparticles embedded in self-healing hydrogels with biocompatible and antibacterial properties, J. Mol. Liq. 310 (2020) 113263, https://doi.org/10.1016/j.molliq.2020.113263.

[12] S.R. Kabir, A.K.M. Asaduzzaman, R. Amin, A.T. Haque, R. Ghose, M.M. Rahman, J. Islam, M.B. Amin, I. Hasan, T. Debnath, B.S. Chun, X.D. Zhao, M.K. Rahman Khan, M.T. Alam, Zizyphus mauritiana fruit extract-mediated synthesized silver/silver chloride nanoparticles retain antimicrobial activity and induce apoptosis in MCF-7 cells through the fas pathway, ACS Omega 5 (2020) 20599–20608, https://doi.org/10.1021/acsomega.0c02878.

[13] S.H. Prakash, S. Rajeshkumar, M.A. Khan, C.S. Prabu, M.R. Khan, E. Arunkumar, S. M. Roopan, Enhancing fruit preservation: fungal growth inhibition with grape seed-mediated Ag@AgCl nanoparticles through desirability-based optimization, ChemistrySelect 9 (2024), https://doi.org/10.1002/slct.202304485.

[14] M. Zhou, X. Hu, X. Xu, Y. Jing, Y. Lai, S. Su, S. Mahmud, X. Zhang, J. Zhu, Controlled synthesis of silver/silver chloride composite crystals from [AgCl2]-complex and its photocatalysis properties on organic pollutants, Colloids Surf. A Physicochem. Eng. Asp. 647 (2022) 128984, https://doi.org/10.1016/j.colsurfa.2022.128984.

[15] A. Dutta, A. Matikainen, S. Andoh, T. Nuutinen, SERS activity of photoreduced silver chloride crystals, AIP Conf. Proc. 2220 (2020), https://doi.org/10.1063/5.0001101.

[16] W. Xu, Z. Wang, P. Liu, X. Tang, S. Zhang, H. Chen, Q. Yang, X. Chen, Z. Tian, S. Dai, L. Chen, Z. Lu, Ag nanoparticle-induced surface chloride immobilization strategy enables stable seawater electrolysis, Adv. Mater. 36 (2024) 1–8, https://doi.org/10.1002/adma.202306062.

[17] W. Fu, W. Yang, C. Qian, Y. Fu, Y. Zhu, One-pot synthesis of Ag/AgCl heterojunction nanoparticles on polyaniline nanocone arrays on graphene oxide for microwave absorption, ACS Appl. Nano Mater. 6 (2023) 3728–3737, https://doi.org/10.1021/acsanm.2c05440.

[18] K. Bhattacharjee, B.L.V. Prasad, Surface functionalization of inorganic nanoparticles with ligands: a necessary step for their utility, Chem. Soc. Rev. 2573-2595 (52) (2023) 2573–2595, https://doi.org/10.1039/D1CS00876E.

[19] A. Gibała, P. Żeliszewska, T. Gosiewski, A. Krawczyk, D. Duraczyńska, J. Szaleniec, M. Szaleniec, M. Oćwieja, Antibacterial and antifungal properties of silver nanoparticles—effect of a surface-stabilizing agent, Biomolecules 11 (2021) 1–20, https://doi.org/10.3390/biom11101481.

[20] F. Wu, D. Liu, T. Wang, W. Li, X. Zhou, Different surface properties of l-arginine functionalized silver nanoparticles and their influence on the conductive and adhesive properties of nanosilver films, J. Mater. Sci. Mater. Electron 26 (2015) 6781–6786, https://doi.org/10.1007/s10854-015-3289-4.

[21] L.B. Wright, N.A. Merrill, M.R. Knecht, T.R. Walsh, Structure of arginine overlayers at the aqueous gold interface: implications for nanoparticle assembly, ACS Appl. Mater. Interfaces 6 (2014) 10524–10533, https://doi.org/10.1021/am502119g.

[22] S. Agnihotri, G. Bajaj, S. Mukherji, S. Mukherji, Arginine-assisted immobilization of silver nanoparticles on ZnO nanorods: an enhanced and reusable antibacterial substrate without human cell cytotoxicity, Nanoscale 7 (2015) 7415–7429, https://doi.org/10.1039/c4nr06913g.

[23] K. Wang, Z. Qi, S. Pan, S. Zheng, H. Wang, Y.X. Chang, H. Li, P. Xue, X. Yang, C. Fu, Preparation, characterization and evaluation of a new film based on chitosan, arginine and gold nanoparticle derivatives for wound-healing efficacy, RSC Adv. 10 (2020) 20886–20899, https://doi.org/10.1039/d0ra03704d.

[24] Z. Shu, J. Li, N. Mu, Y. Gao, T. Huang, Y. Zhang, Z. Wang, M. Li, Q. Hao, W. Li, L. He, C. Zhang, W. Zhang, X. Xue, Y. Zhang, Expression, purification and characterization of galectin-1 in Escherichia coli, Protein Expr. Purif. 99 (2014) 58–63, https://doi.org/10.1016/j.pep.2014.03.013.

[25] D.C. Kennedy, G. Orts-Gil, C.H. Lai, L. Müller, A. Haase, A. Luch, P.H. Seeberger, Carbohydrate functionalization of silver nanoparticles modulates cytotoxicity and cellular uptake, J. Nanobiotechnol. 12 (2014) 1–8, https://doi.org/10.1186/s12951-014-0059-z.

[26] S. Sancak, İ. Yazgan, A.U. Bayarslan, A. Ayna, S. Evecen, Z. Taşdelen, A. Gümüş, H. A. Sönmez, M.A. Demir, S. Demir, F. Bakar, H. Dilek-Tepe, K. Kasemets, M. Otsus, T. Çeter, Surface chemistry dependent toxicity of inorganic nanostructure glycoconjugates on bacterial cells and cancer cell lines, J. Drug Deliv. Sci. Technol. 79 (2023), https://doi.org/10.1016/j.jddst.2022.104054.

[27] H.F. Hetta, Y.N. Ramadan, A.I. Al-Harbi, E. A. Ahmed, B. Battah, N.H. Abd Ellah, S. Zanetti, M.G. Donadu, Nanotechnology as a promising approach to combat multidrug resistant bacteria: a comprehensive review and future perspectives, Biomedicines 11 (2023) 413, https://doi.org/10.3390/biomedicines11020413.

[28] I. Yazgan, A. Gümüş, K. Gökkuş, M.A. Demir, S. Evecen, H.A. Sönmez, R.M. Miller, F. Bakar, A. Oral, S. Popov, M.S. Toprak, On the effect of modified carbohydrates on the size and shape of gold and silver nanostructures, Nanomaterials 10 (2020) 1–17, https://doi.org/10.3390/nano10071417.

[29] K. Katagiri, T. Ikeda, M. Tominaga, H. Masu, I. Azumaya, Coordination polymers and networks constructed from bidentate ligands linked with sulfonamide and silver(I) ions, Cryst. Growth Des. 10 (2010) 2291–2297, https://doi.org/10.1021/cg100013g.

[30] H.C. Schwarzer, W. Peukert, Combined experimental/numerical study on the precipitation of nanoparticles, AIChE J. 50 (2004) 3234–3247, https://doi.org/10.1002/aic.10277.

[31] M. Tepe, M.S. Zeybek, Chemistry of plant extracts directs the silver nanostructures' crystal structure into hexagonally close-packed: a comparative study using elecampane and blueberry extracts, Anadian J. Chem. 102 (2024) 431–447, https://doi.org/10.1139/cjc-2023-022.

[32] S. Rajendran, Corrosion behaviour of carbon steel in isoelectric point and nearly neutral aqueous medium by L – arginine and zinc ion as a synergist, 2016.

[33] R. Tandiana, C. Sicard-Roselli, N.T. Van-Oanh, S. Steinmann, C. Clavaguéra, In-depth theoretical understanding of the chemical interaction of aromatic compounds with a gold nanoparticle, Phys. Chem. Chem. Phys. 24 (2022) 25327–25336, https://doi.org/10.1039/d2cp02654f.

[34] C. Pattnaik, R. Mishra, A. Lenka, B.P. Kar, S.K. Dash, L.N. Sahoo, S.K. Tripathy, G. C. Nayak, S. Sahoo, Exploring the versatility of carbohydrate-capped green silver nanoparticles as multi-dimensional reagents for targeted applications, J. Mol. Struct. 1319 (2025) 139544, https://doi.org/10.1016/j.molstruc.2024.139544.

[35] F.E. Gallegos, L.M. Meneses, S.A. Cuesta, J.C. Santos, J. Arias, P. Carrillo, F. Pilaquinga, Computational modeling of the interaction of silver clusters with carbohydrates, ACS Omega 7 (2022) 4750–4756, https://doi.org/10.1021/acsomega.1c04149.

[36] A.W. Orbaek, M.M. McHale, A.R. Barron, Synthesis and characterization of silver nanoparticles for an undergraduate laboratory, J. Chem. Educ. 92 (2015) 339–344, https://doi.org/10.1021/ed500036b.

[37] K.G. Stamplecoskie, J.C. Scaiano, Light emitting diode irradiation can control the morphology and optical properties of silver nanoparticles, J. Am. Chem. Soc. 132 (2010) 1825–1827, https://doi.org/10.1021/ja910010b.

[38] T. Shoeib, K.W.M. Siu, A.C. Hopkinson, Silver ion binding energies of amino acids: Use of theory to assess the validity of experimental silver ion basicities obtained from the kinetic method, J. Phys. Chem. A 106 (2002) 6121–6128, https://doi.org/10.1021/jp013662z.

[39] M. Antonilli, E. Bottari, M.R. Festa, L. Gentile, Potentiometric investigation of silver (I) complexation by arginine, Ann. Chim. 97 (2007) 1257–1267. ⟨http://digilib.unila.ac.id/4949/15/BABII.pdf⟩.

[40] A.P. Co, G.K.H. Shimizu, V. Uni, A. Tn, Silver (I) arylsulfonates: a systematic study of " softer " hybrid inorganic – organic solids, Inorg. Chem. 43 (2004) 6663–6673.

[41] S. Kumar, S.B. Rai, Spectroscopic studies of L-arginine molecule, Indian J. Pure Appl. Phys. 48 (2010) 251–255.

[42] A. Roda, F. Santos, Y.Z. Chua, A. Kumar, H.T. Do, A. Paiva, A.R.C. Duarte, C. Held, Unravelling the nature of citric acid:L-arginine:water mixtures: The bifunctional role of water, Phys. Chem. Chem. Phys. 23 (2021) 1706–1717, https://doi.org/10.1039/d0cp04992a.

[43] M. Wolpert, P. Hellwig, Infrared spectra and molar absorption coefficients of the 20 alpha amino acids in aqueous solutions in the spectral range from 1800 to 500 cm-1, Spectrochim. Acta - Part A Mol. Biomol. Spectrosc. 64 (2006) 987–1001, https://doi.org/10.1016/j.saa.2005.08.025.

[44] A. Barth, The infrared absorption of amino acid side chains, Prog. Biophys. Mol. Biol. 74 (2000) 141–173, https://doi.org/10.1016/S0079-6107(00)00021-3.

[45] A. Küçük, Z. Taşdelen, Ş. Güney, S. Sel, E.İ. Demirbaş, F.Ö. Kırbay, S. Sancak, M. Otsus, H. Dilek-Tepe, K. Kasemets, Ç . Kılınç, İ. Yazgan, Development of inorganic nanoparticle glycoconjugate enhanced cotton fabrics for multi-drug-resistant pseudomonas aeruginosa bacterium, Microbe xxx (2025) 100269, https://doi.org/10.1016/j.microb.2025.100269.

[46] A.A. Buglak, R.R. Ramazanov, A.I. Kononov, Silver cluster–amino acid interactions: a quantum-chemical study, Amino Acids 51 (2019) 855–864, https://doi.org/10.1007/s00726-019-02728-z.

[47] Á.I. López-Lorente, B. Mizaikoff, Recent advances on the characterization of nanoparticles using infrared spectroscopy, TrAC - Trends Anal. Chem. 84 (2016) 97–106, https://doi.org/10.1016/j.trac.2016.01.012.

[48] S.P. Schwaminger, P.F. García, G.K. Merck, F.A. Bodensteiner, S. Heissler, S. Günther, S. Berensmeier, Nature of interactions of amino acids with bare magnetite nanoparticles, J. Phys. Chem. C 119 (2015) 23032–23041, https://doi.org/10.1021/acs.jpcc.5b07195.

[49] I. Yazgan, A. Gümü, S. Popov, M.S. Toprak, On the effect of modified carbohydrates on the size and shape of gold and silver nanostructures, Nanomaterials 10 (2020) 1–17, https://doi.org/10.3390/nano10071417.

[50] A.S. Santhosh, S. Sandeep, H.M. Manukumar, B. Mahesh, N. Kumara Swamy, Green synthesis of silver nanoparticles using cow urine: Antimicrobial and blood biocompatibility studies, JCIS Open 3 (2021) 100023, https://doi.org/10.1016/j.jciso.2021.100023.

[51] Y. Zhu, H. Liu, L. Yang, J. Liu, Study on the synthesis of Ag/AgCl nanoparticles and their photocatalytic properties, Mater. Res. Bull. 47 (2012) 3452–3458, https://doi.org/10.1016/j.materresbull.2012.07.005.
[52] M. Choi, K.H. Shin, J. Jang, Plasmonic photocatalytic system using silver chloride/silver nanostructures under visible light, J. Colloid Interface Sci. 341 (2010) 83–87, https://doi.org/10.1016/j.jcis.2009.09.037.
[53] S. Glaus, G. Calzaferri, Silver chloride clusters and surface states, J. Phys. Chem. B 103 (1999) 5622–5630, https://doi.org/10.1021/jp990701m.
[54] H.D. Tepe, Ş. Aktaş, T. Çeter, İ. Yazgan, Comparison of blueberry and dandelion aqueous extracts in the synthesis of gold and silver nanostructures, and their applications as anti-pseudomonas aeruginosa agent, ChemistrySelect 8 (2023) e202300362, https://doi.org/10.1002/slct.202300362.
[55] M. Grouchko, I. Popov, V. Uvarov, S. Magdassi, A. Kamyshny, Coalescence of silver nanoparticles at room temperature: unusual crystal structure transformation and dendrite formation induced by, Langmuir (2016) 2501–2503.
[56] I. Chakraborty, S.N. Shirodkar, S. Gohil, U.V. Waghmare, P. Ayyub, The nature of the structural phase transition from the hexagonal (4H) phase to the cubic (3C) phase of silver, J. Phys. Condens. Matter 26 (2014) 115405, https://doi.org/10.1088/0953-8984/26/11/115405.
[57] Y. Liu, K. Yang, H. Zhang, Y. Jia, Z. Wang, Combating antibiotic tolerance through activating bacterial metabolism, Front. Microbiol 11 (2020), https://doi.org/10.3389/fmicb.2020.577564.
[58] S.I. Hossain, D. Bajrami, N. Altun, M. Izzi, C.D. Calvano, M.C. Sportelli, L. Gentile, R.A. Picca, P. Gonzalez, B. Mizaikoff, N. Cioffi, Development of super nanoantimicrobials combining AgCl, tetracycline and benzalkonium chloride, Discov. Nano 19 (2024), https://doi.org/10.1186/s11671-024-04043-3.
[59] Optimized broth microdilution plate methodology for drug susceptibility testing of Mycobacterium tuberculosis complex, Geneva, 2022.
[60] S. Ramanathan, D. Ravindran, K. Arunachalam, Inhibition of quorum sensing-dependent biofilm and virulence genes expression in environmental pathogen Serratia marcescens by petroselinic acid, Antonie Van. Leeuwenhoek 111 (2018) 501–515, https://doi.org/10.1007/s10482-017-0971-y.
[61] F. Gui, W. Mo, X. Guo, F. Cao, T. Zhai, C. Hong, X. Guan, B. Huang, X. Pan, Biosynthesis of nanocrystalline silver chloride with high antibacterial activity using bacterial extracts, Adv. Agrochem. 2 (2023) 88–96, https://doi.org/10.1016/j.aac.2022.12.002.